A Comparison Between Fully-Unsteady and Quasi-Steady Approach for the Prediction of the Propeller Performance in Waves

Simone Saettone[*,†], Bhushan Taskar[*], Pelle Bo Regener[*], Sverre Steen[†], and Poul Andersen[*]

[*] *Technical University of Denmark, Kgs. Lyngby, Denmark*

[†] *Norwegian University of Science and Technology, Trondheim, Norway*

Abstract

Maritime transport is the most energy-effective mode to move large amounts of goods around the world. Hauling cargo via waterway produces an enormous quantity of greenhouse gas emissions. Vessel fuel efficiency directly influences ship emissions by affecting the amount of burnt fuel. Optimizing ships operating in waves rather than in calm water conditions could decrease the fuel consumption of vessels. In particular, ship propellers are traditionally designed neglecting dynamic conditions such as time-varying wake distribution and propulsion factors, propeller speed fluctuations, ship motions, and speed loss.

The effect of waves on the propeller performance can be evaluated using both a quasi-steady and a fully-unsteady approach. The former is a fast computational approximation method based on the assumption that the ratio of propeller angular frequency to wave encounter frequency is sufficiently large. The latter provides a complete representation of the propeller dynamics, but it is computationally expensive.

The purpose of this paper is to compare the propeller performance in the presence of waves using the quasi-steady and the fully unsteady approach. This analysis is performed by observing the differences in unsteady propeller forces, cavitation volume, and hull pressure pulses between the two approaches. The full-scale KVLCC2 propeller is utilized for the investigation.

Results show a good agreement between the quasi-steady and the fully-unsteady approach in the prediction of the temporal mean and the fluctuation amplitude of K_T and K_Q, the cavity volume variation, and the hull pressure pulses. Therefore, for the considered operating conditions,

the quasi-steady approach can be used to compute the propeller performance in waves.

Keywords: Propulsion in waves, Ship Propeller, Cavitation, Pressure pulses

---

Nomenclature

A	Wave amplitude
C_F	Friction resistance coefficient
C_P	Pressure coefficient
C_R	Residual resistance coefficient
D	Propeller diameter
h	Shaft submergence
H	Wave height
J	Advance ratio
J_{calm}	Advance ratio in calm water
J_{wave}	Averaged advance ratio in waves
K_Q	Torque coefficient
K_T	Thrust coefficient
L_{PP}	Length between perpendiculars
n	Propeller rate of revolutions
P	Pressure over the propeller blade
R	Propeller radius
t	Time instance
T_e	Encounter wave period
U	Ship speed
V_f	Fluctuating wake velocity due to waves
V_m	Mean wake velocity due to waves
V_t	Total wake velocity due to waves
w_w	Full-scale effective average wake fraction in waves
W_c	Wake distribution in calm water
W_{pc}	Potential part of the wake distribution in calm water
W_{pw}	Potential part of the wake distribution in waves
W_w	Wake distribution in waves
ρ	Water density

ω_e	Encounter wave frequency
ω_{prop_c}	Computed propeller angular frequency in calm water conditions
ω_{prop_d}	Design propeller angular frequency
λ	Wavelength

1. Introduction

Maritime transport is of great importance to the global economy as over 90% of the world's trade is carried via waterway [23]. However, the shipping industry emits in total around 940 million tonnes of CO_2 annually, and it is responsible for about 2.5% of global greenhouse gas emissions [25]. The United Nations International Maritime Organization (IMO) has recently developed a strategy to reduce the total annual greenhouse gas emissions by at least 50% by 2050 compared to 2008.

Ships are traditionally optimized in ideal conditions where waves, wind, and currents are taken care of by simply adding a margin to the estimation of the speed-power relationship for a newly built vessel in trial conditions. This can be explained by insufficient tools and knowledge to optimize ships in realistic operating conditions. Nevertheless, measurements performed on ships operating in waves indicate a significant change in fuel consumption because of the reduced propulsive efficiency, e.g. [2]. Therefore, more energy-efficient ships can be designed if dynamic conditions are taken into account during the optimization phase.

Ship propellers are usually designed without considering the time-variation of wake distribution and propulsion factors and neglecting propeller speed fluctuations, speed loss, and ship motions. However, unsteady RANS simulations performed by Guo et al. [5] indicated that axial velocities at the propeller disk could increase up to 35% of the ship forward speed in the presence of waves. Kim et al. [12] showed the fluctuation of propeller plane wake by measuring the phase-averaged flow field in waves around the KVLCC2 tanker using a SPIV system. Similarly, Sadat-Hosseini et al. [24] measured the time-variation of velocity distribution at the propeller plane in waves for the KVLCC2 ship with a PIV system. Results of experiments performed by Moor and Murdey [19] and Nakamura and Naito [20] showed that the propulsion factors vary significantly in the presence of waves. In addition, Jessup and Wang [11] and Chevalier and Kim [1] observed a reduction in cavitation inception speed with respect to calm water conditions. Taskar et al. [29] [30] studied the change in propeller performance in the presence of waves in terms of cavitation, hull pressure pulses, and efficiency. It was found out that

time-varying wake field and shaft submergence, propeller speed fluctuations, and speed loss contribute the most to the variation of propeller performance compared to calm water conditions. Taskar et al. [31] studied different aspects of the propulsion system of the KVLCC2 tanker in the time-varying wake field in waves. It was observed that the time-varying wake field gives rise to fluctuating loads on the propeller, which leads to a time-variation of the shaft speed and engine torque. Taskar et al. [29] [30] [31] treated the variation of inflow caused by waves and ship motions in a quasi-steady manner, meaning that the flow field entering the propeller disk was treated as time-invariant for each time instant. Steen and Chuang [26] provided an overview of the physical effects contributing to speed loss. It was discussed how added resistance, ventilation, propeller out-of-water, wave-making by the propeller due to closeness to free surface, change of propulsive factors and propulsion point cause involuntary ship speed loss. It is also well known that wave-induced ship motions lead to a fluctuation of propeller immersion and, consequently, to a time-varying cavitation number. Time-varying propeller speed, wave-induced ship motions, and speed loss affect the propeller efficiency, influence the propeller cavitation pattern and cause an increase in propeller-induced pressure pulses [28].

The effect of waves on the propeller performance can be evaluated using both a quasi-steady, e.g. [29] [30] [31], and a fully-unsteady approach. In the former, time-varying input data, such as wake distribution, propulsion factors, propeller speed fluctuations, and ship motions, are only known for a number of time instances sufficient to reproduce the wave phenomenon accurately in time. For each time instant, one unsteady simulation is run where the corresponding time-varying input data are kept constant in time throughout the time-dependent calculation. The unsteadiness of the results is only related to the spatial non-uniformity of the wake distribution because the time-varying input data are fixed in time for each simulation. Each quasi-steady calculation provides results only at the selected time instance. After collecting the results, it is possible to obtain a trend in time for the propeller performance for the entire wave period. This method is computationally fast, and it can be carried out by any kind of potential flow code able to compute unsteady propeller performance. This is because the time-varying input data are time-invariant in each time-dependent calculation for both calm water conditions and waves. On the other hand, the quasi-steady approach completely neglects the time history of the propeller performance related to the time-varying input data. For instance, the evolution in time

of the velocity potential shed into the blade wake is based on a time-invariant wake field and propeller speed. This approximation is considered acceptable because the ratio of propeller angular frequency to wave encounter frequency is sufficiently large. However, the validity of the quasi-steady approach is currently not known. The propeller performance should be computed by applying the fully-unsteady approach, where the time history of the time-varying input data is taken into account. This is performed, ideally, by running only one unsteady simulation where the time-varying input data are changing in time during the unsteady computation. However, the fully-unsteady approach is computationally expensive compared to the quasi-steady approach.

The purpose of this paper is to compare the propeller performance in the presence of waves using the quasi-steady and the fully unsteady approach. This is carried out in two steps:

1. **Open water condition**. This is a simple study performed to obtain a quick insight into the differences in unsteady propeller forces between the quasi-steady and the fully-unsteady approach. The time-varying wake field is simply generated by a plane progressive wave in open water conditions. Propeller speed fluctuations and ship motions are neglected. This study is carried out in non-cavitating conditions.
2. **Behind ship condition**. This study is performed to confirm the results obtained from the previous step by considering realistic case scenarios. This comparison takes into account time-varying wake distribution and shaft submergence, propeller speed fluctuations, and speed loss. The differences in unsteady propeller forces, hull pressure pulses, and cavitation volume between the quasi-steady and the fully-unsteady approach are computed.

2. Propeller analysis

The propeller analysis is performed applying both the fully-unsteady and the quasi-steady approach. Figure 1 shows the different algorithms implemented in the present paper for the two methods. Several independent simulations are necessary to estimate the propeller performance for the entire wave phenomenon with the quasi-steady approach. On the other hand, two simulations, one in non-cavitating conditions and one in cavitating conditions (see Section 2.2), are necessary for the fully-unsteady approach.

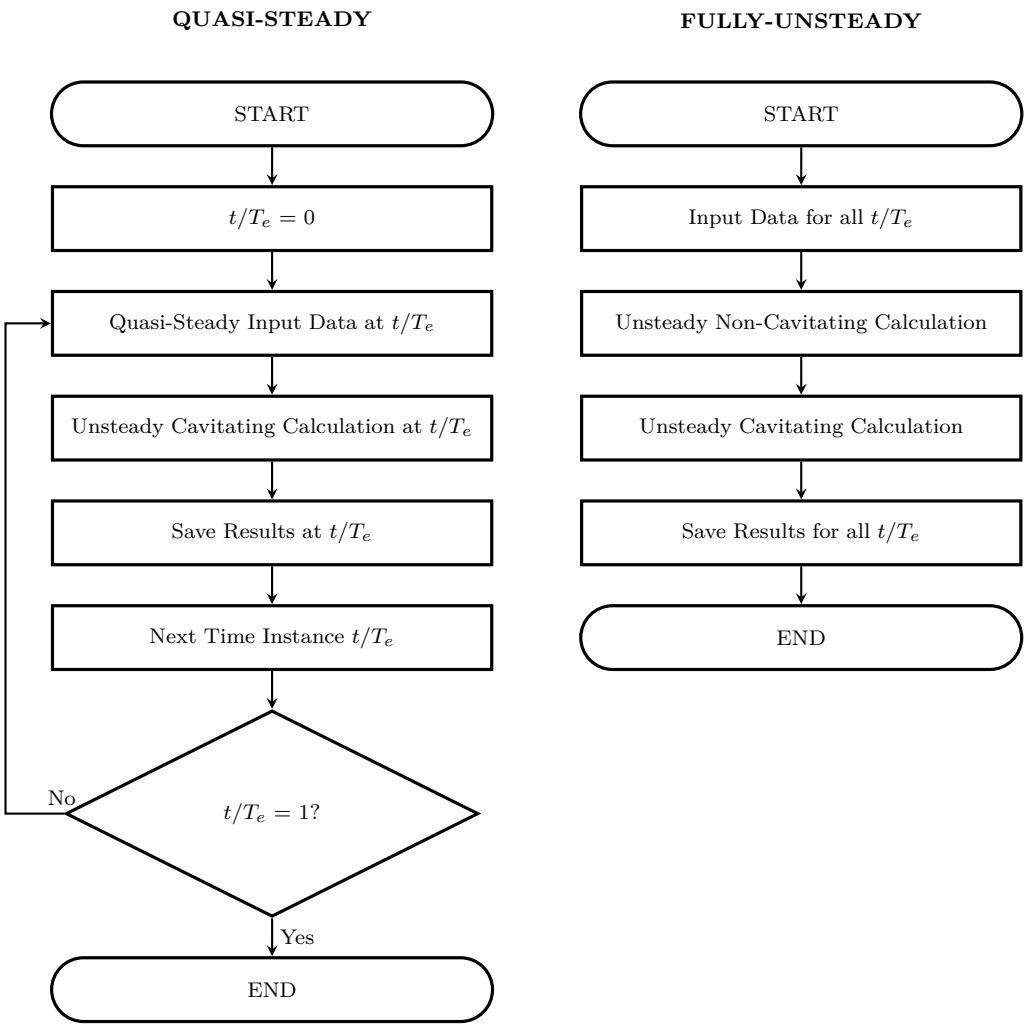

Figure 1: Algorithm comparison: quasi-steady vs fully-unsteady approach.

2.1. Propeller model: ESPPRO

The DTU-developed unsteady low-order boundary-element method ESPPRO [21] serves as the main tool for the propeller analysis. It is based on potential flow formulation where the flow is assumed to be inviscid, incompressible, and irrotational. The boundary-element method, compared to other potential flow numerical methods, provides a complete representation of the propeller geometry by placing the distribution of source and dipole singularities on the actual propeller surface.

ESPPRO was validated against results reported for similar methods for ship propellers, such as [35] and [34]. Additionally, Mirsadraee [17] showed the good agreement, in terms of propeller performance and cavitation behavior, between experimental data and ESPPRO results for the KRISO container ship propeller (KCS) [13].

The propeller blades are discretized into 40 panels in both spanwise and chordwise direction. Cosine stretching is applied for the latter and equidistant stretching for the former (see Appendix A).

In the present work, ESPPRO is modified to take into account of time-varying wake field and shaft submergence and propeller speed fluctuations in a fully-unsteady manner. The main modifications are related to the cavitation model (Section 2.2) and the blade wake model (Section 2.3).

2.2. Cavitation model

The sheet cavitation model implemented in ESPPRO is described by Regener et al. [22]. The implementation derives from the method initially introduced by Kinnas and Fine [14]. ESPPRO can predict unsteady sheet cavitation, including supercavitation, in also inhomogeneous inflow. In calm water conditions, the cavitation model is activated after at least one full revolution in the non-cavitating condition where the unsteady terms are stored internally at every time step. These saved time-derivatives are applied on the wetted part of the blade when the cavitation model is activated. This simplification can be applied because of the periodicity of the unsteady terms. However, in the presence of waves, the unsteady terms are not periodic because wave frequency and blade frequency are, generally, not multiples of each other. As a consequence, the previous technique cannot be applied to the fully-unsteady approach. An efficient solution consists of running first the propeller model in non-cavitating conditions and then compute another simulation where the cavitation model is activated. The former is only necessary to store the

unsteady terms externally at every time step. The latter computes the propeller performance, where the unsteady terms saved in the first simulation are used. This technique solves quickly the problem related to the non-periodicity of the unsteady terms without performing significant modifications to the software. As a disadvantage, two completely different simulations are required to compute the propeller performance in waves.

2.3. Blade wake model

Three blade-wake models are currently available in ESPPRO:

1. A blade wake alignment model inspired by Tian and Kinnas [32]. In this model, the trailing vortex sheets of the blades are aligned with the local flow velocity. Slipstream contraction and other complex phenomena are taken into account.
2. A geometry for the blade wake inspired by Hoshino [6]. This blade model takes into account the contraction of the slipstream and the variation of the pitch of helical trailing vortex sheets.
3. A geometry for the blade wake inspired by Streckwall [27]. This simple blade wake model accounts for neither roll-up of the tip vortex nor slipstream contraction. The blade pitch is a function of both blade pitch at r/R = 0.9 and advance ratio.

The first blade wake model provides the best comparison with KVLCC2 experimental open water data [18]. However, it is computationally expensive, especially for long-time simulations with small time steps as in the presence of waves. The open water characteristics computed by ESPPRO with the third wake blade model show a better agreement with the experimental open water data than the second wake blade model. Therefore, even though it is comparatively simple, the wake model inspired by Streckwall [27] is applied in the current work for both the quasi-steady and the fully-unsteady approach.

Typically, for this type of model, the blade wake geometry is "frozen" during the unsteady simulation since the advance ratio is constant in time. However, in the presence of waves, propeller speed fluctuations and time-varying wake field lead to a time-variation of the advance ratio. Thus, the blade wake geometry needs to be reconstructed, at every time step, by recomputing the blade wake pitch for the fully-unsteady approach. In the quasi-steady approach, the blade wake geometry is still "frozen" in time because, for each simulation, propeller speed and wake field are time-invariant.

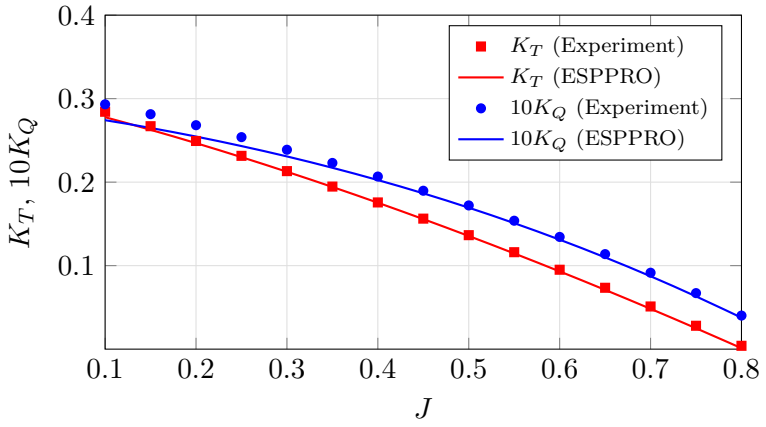

Figure 2: Open Water Diagram for the MOERI KP458 propeller.

3. Case vessel

The full-scale KVLCC2 tanker with the MOERI's corresponding propeller, see Table 1 and 2 or Kim et al. [13], are utilized in the present case study.

Length between perpendiculars	320.0 m
Breadth	58.0 m
Design draft	20.8 m
Design shaft submergence	15.1 m
Service speed	15.5 kts

Table 1: KVLCC2 main particulars.

Diameter	9.86 m
Design propeller speed	76 rpm
Number of blades	4
A_E/A_O	0.431
$(P/D)_{\text{Mean}}$	0.690

Table 2: KP458 propeller characteristics.

4. Open water condition

Seven plane progressive waves in head sea conditions are considered. Wave characteristics are shown in Table 3. For simplicity, the presence of the ship is neglected, and the propeller performance are computed in non-cavitating conditions.

The propeller inflow, for the quasi-steady approach, is computed at eleven time instances, t, in one encounter wave period, T_e, for each plane progressive wave. At $t/T_e = 0.75$ the time-varying average wake fraction has its maximum value for each wave.

The temporal resolution selected for the fully-unsteady approach is set equal to 0.004 seconds. This fine time step is necessary for the accuracy of

Wave [−]	H/λ [−]	A [m]	λ/L_{PP} [−]	ω_e [rad/sec]	ω_{prop_d}/ω_e [−]
OW_1	0.040	1.123	0.176	1.667	4.77
OW_2	0.040	1.529	0.239	1.353	5.88
OW_3	0.040	1.997	0.312	1.134	7.02
OW_4	0.040	2.527	0.395	0.974	8.17
OW_5	0.040	3.120	0.488	0.851	9.35
OW_6	0.040	3.775	0.590	0.756	10.53
OW_7	0.040	4.493	0.702	0.679	11.73

Table 3: Open water condition - Wave characteristics.

the approach. The propeller inflow is obtained by B-spline interpolation of the wake field computed for the quasi-steady approach.

Propeller speed fluctuations and ship motions are neglected. Shaft submergence and propeller speed are assumed to be constant in time and set equal to their design values.

4.1. Method

The time-varying wake field in waves is generated by a regular sinusoidal propagating wave in infinite water depth. The wave velocities are computed as described by Faltinsen [3].

The time-invariant part of the propeller inflow velocity is adjusted to set the advance ratio in open water conditions equal to the full-scale calm water advance ratio calculated by Kim et al. [13].

For brevity, the time-varying wake field in waves at the propeller plane, computed by the described method, is shown in Figure 3 only at four time instances for one plane progressive wave.

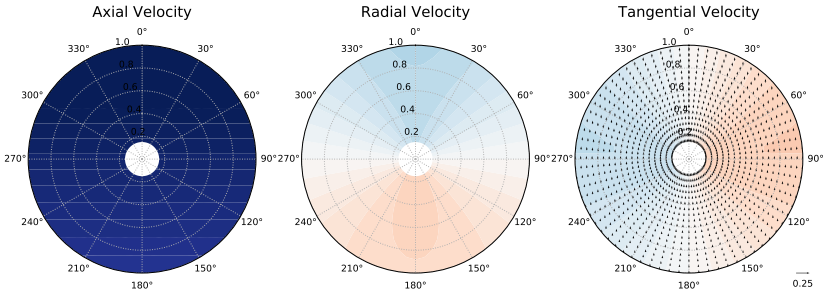

(a) OW_5 - $t/T_e = 0.2$

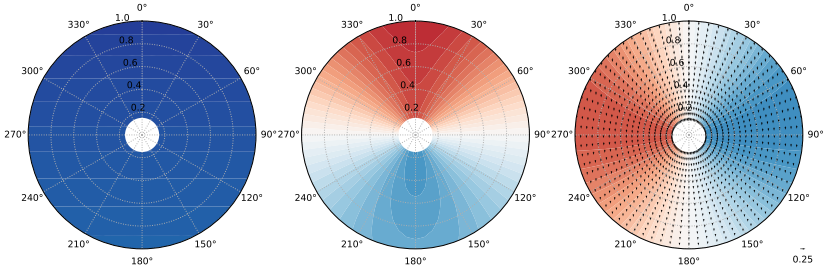

(b) OW_5 - $t/T_e = 0.4$

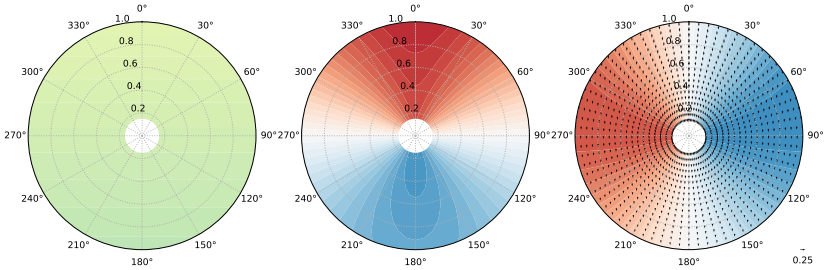

(c) OW_5 - $t/T_e = 0.6$

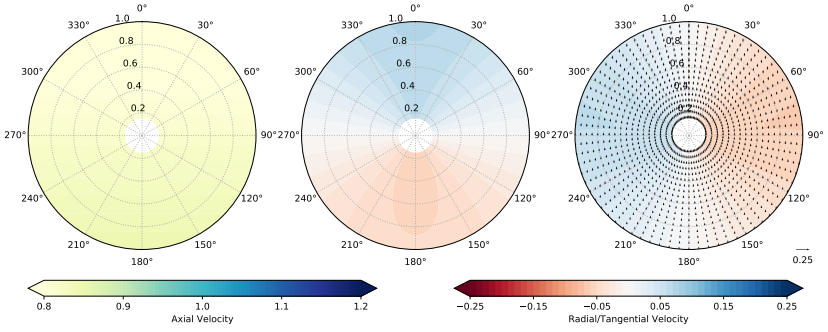

(d) OW_5 - $t/T_e = 0.8$

Figure 3: Open water condition - Time-varying wake field.

5. Behind ship condition

Three regular waves in head sea conditions are considered. Wave characteristics are shown in Table 4.

Wake field, ship motions, and propeller speed fluctuations are computed at eleven time instances, t, in one encounter wave period, T_e, for each regular wave. At $t/T_e = 0$ the time-varying average wake fraction has its minimum value for each wave.

The temporal resolution selected for the fully-unsteady approach is set equal to 0.004 seconds. This fine time step is necessary for the accuracy of the approach. Wake field, ship motions, and propeller speed fluctuations are obtained by B-spline interpolation of the corresponding values computed for the quasi-steady approach.

Hull pressure pulses are evaluated at nine points on a horizontal plane located above the propeller (see Figure 4).

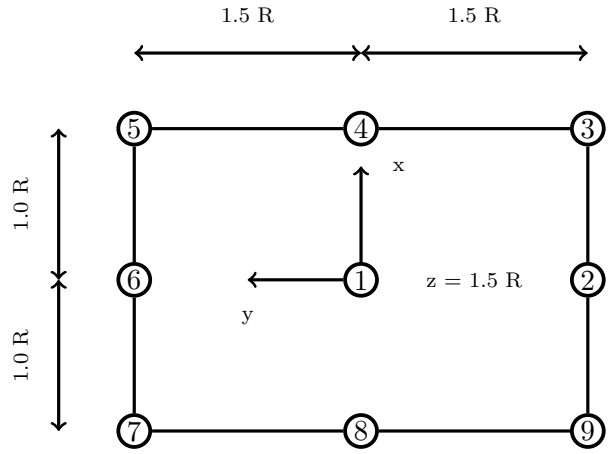

Figure 4: Behind ship condition - Hull pressure points are described in a ship-fixed coordinate system located in the propeller center where the x-axis is positive upstream, the y-axis is positive to the port side, and the z-axis completes the right-hand coordinate system.

Wave [−]	H/λ [−]	H [m]	λ/L_{PP} [−]	ω_e [rad/sec]	ω_{prop_c}/ω_e [−]
BS_1	0.031	3.0	0.6	0.83	8.94
BS_2	0.017	3.0	1.1	0.56	13.19
BS_3	0.012	3.0	1.6	0.44	16.62

Table 4: Behind ship condition - Wave characteristics.

5.1. Method

The comparison between the quasi-steady and the fully-unsteady approach has to be conducted by considering realistic ship operating conditions. However, the limited availability of wake data for ships in waves constitutes an obstacle for this purpose. Therefore, an approximated method (see Figure 5) is applied to determine the realistic time-varying input data (full-scale effective wake field in waves, propeller speed fluctuations, and shaft submergence) and the ship speed in waves. The accuracy of this method is considered sufficient to determine the necessary input for the comparison between the fully-unsteady and the quasi-steady approach behind ship conditions. Therefore, it is necessary to point out that this simple method does not provide the exact time-varying input data for the entire history of a ship sailing in waves. In particular, the time-varying input data are estimated as described by Taskar [28], and the classical power prediction approach is applied to compute the speed loss.

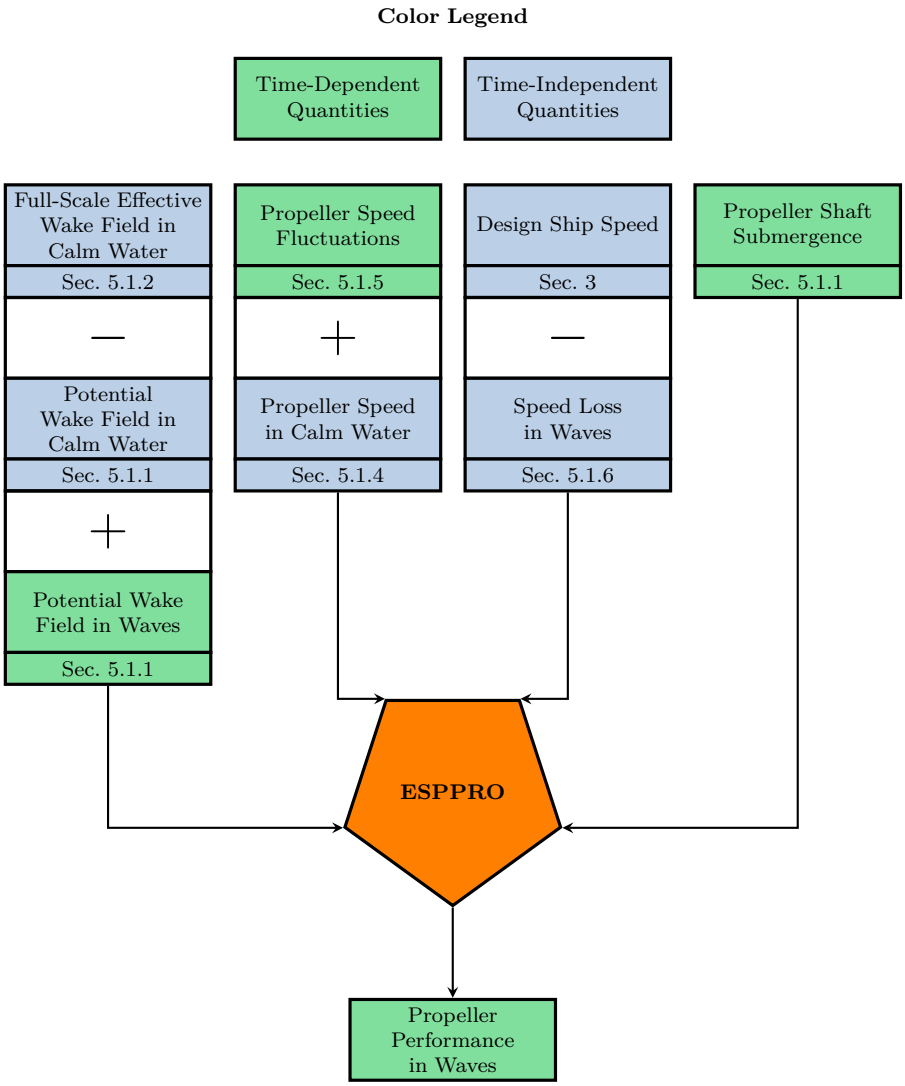

Figure 5: Outline of the estimated input data for the propeller analysis.

5.1.1. Potential wake field and ship motions

The potential wake field in waves and calm water and the ship motions computed by Taskar et al. [31], at the design speed of the ship, are used in the present work. The potential wake fields are necessary to estimate the full-scale effective wake field in waves (see Section 5.1.3).

In the presence of waves, the fully nonlinear, unsteady, three-dimensional boundary-element method implemented in the commercial software SHIPFLOW Motions was used to compute the time-varying propeller shaft submergence and the potential wake field in waves. The numerical model and mathematical method employed in SHIPFLOW Motions are described by Kjellberg [15]. In these simulations, the model was free to heave and pitch, but it was not allowed to surge.

The nonlinear three-dimensional panel method implemented in the commercial software SHIPFLOW-XPAN [10] was utilized to compute the potential wake field in calm water conditions.

The potential wake field in calm water conditions, at the propeller plane, is shown in Figure 6. The potential wake field in waves, also at the propeller plane, is shown in Figure 7. For brevity, the potential wake field in waves is shown only at one time instance for each wave. The time-varying shaft submergences are shown in Figure 8.

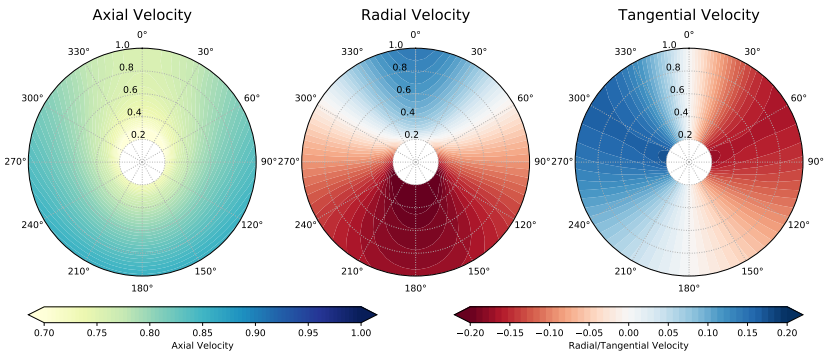

Figure 6: Potential wake field in calm water conditions.

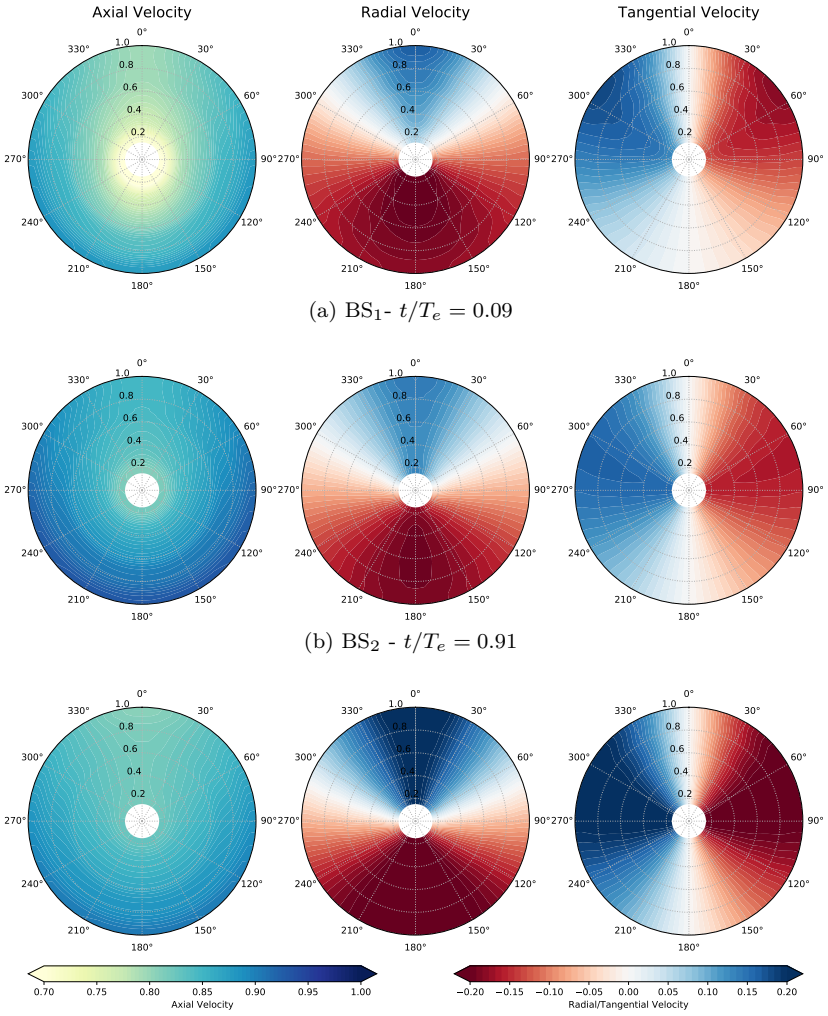

(a) BS_1- $t/T_e = 0.09$

(b) BS_2 - $t/T_e = 0.91$

(c) BS_3 - $t/T_e = 0.79$

Figure 7: Time-varying potential wake field in waves.

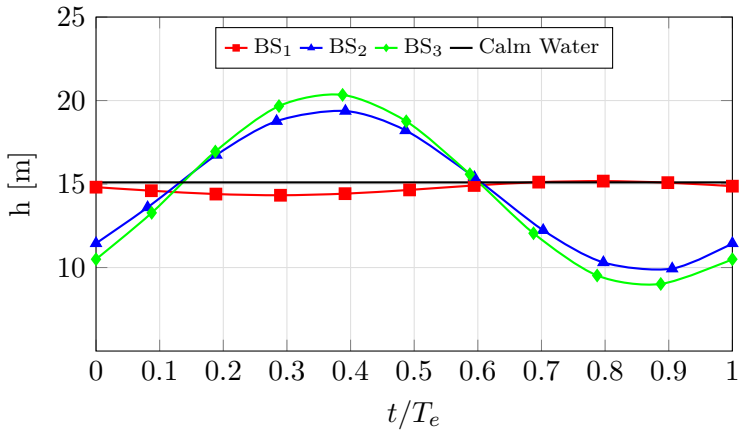

Figure 8: Time-varying shaft submergences in waves.

5.1.2. Full-scale effective wake field in calm water

The full-scale effective wake field in calm water, at the design speed of the ship, is computed using the RANS-BEM coupling approach described and validated by Regener [21]. The full-scale effective wake field in calm water is necessary to estimate the full-scale effective wake field in waves (see Section 5.1.3).

In the RANS-BEM coupling approach, the hull flow is solved with a Reynolds-averaged Navier-Stokes (RANS) solver, and a boundary-element method (BEM) is applied for the propeller analysis. The blade blockage effect is addressed as explained by Regener et al. [22]. The effective velocity field is computed in a plane located upstream of the propeller, following the contour of the blade's leading edge at an upstream distance of 5% of the propeller radius. The free surface is not included in the simulation (double body approach). Other details of the RANS-BEM computational set-up can be found in Regener [21].

In the present work, the DTU-developed unsteady low-order panel code ESPPRO is used on the BEM side (see Section 2). The viscous flow solver XCHAP, from the commercial software SHIPFLOW package, is used on the RANS side. XCHAP solves the Reynolds Averaged Navier-Stokes equations using the EASM (Explicit algebraic stress model) turbulence model. The RANS equations are discretized using a finite volume method (FVM) on multi-block overlapping grids. The same SHIPFLOW computational set-up as implemented by Larsson et al. [16] is applied in the present study (apart from the necessary differences from model to full scale). The fine and body-fitted computational grid around the hull is further refined towards the ship stern to resolve correctly the propeller plane flow. For simplicity, a comparison of the computed wake distribution with the velocity fields estimated by other turbulence models is not carried out. This is because, as explained in Section 5.1, the method applied to determine the time-varying input data is not intended to provide the exact time-varying wake distribution of a ship sailing in waves.

The full-scale effective wake field in calm water conditions, computed coupling ESPPRO with SHIPFLOW, is shown in Figure 9. Details of the grid implemented in the RANS simulation are shown in Appendix B. The propeller grid utilized in the BEM computation can be seen in Appendix A. The suction side pressure distribution over the propeller blade is presented in Appendix C.

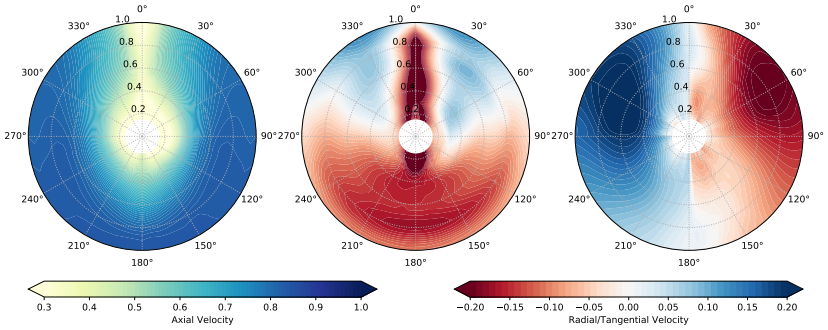

Figure 9: Full-scale effective wake field in calm water.

5.1.3. Full-scale effective wake field in waves

The full-scale effective wake field in waves, necessary for the propeller analysis, is computed, at the design speed of the ship, by following the method described by Taskar et al. [31]. The main idea behind this approach is to estimate the wake field distribution in the presence of waves by decomposing the wake field, at any point in time, into a time-varying and time-invariant wake field. The assumption is that the former can be described by the potential part of the wake field and the latter by the viscous part of the wake field. Therefore, the assumption is that the wake variation due to waves is primary due to potential effects, even though the wake itself is a viscous phenomenon. Consequently, the potential part of the wake distribution in calm water W_{pc} (see Section 5.1.1) is subtracted from the total wake distribution in calm water W_c (see Section 5.1.2), and then the potential part in waves W_{pw} (see Section 5.1.1) is added:

$$W_w = W_c - W_{pc} + W_{pw}$$

Taskar et al. [31] applied this approach to predict the nominal wake field of the KVLCC2 tanker in model-scale. The potential wake field was computed with the procedure explained in Section 5.1.1. The comparison showed that the wake obtained using the method did not resemble the wake distribution determined by CFD simulations [24]. According to Taskar et al. [31], the main reason for this result is that, in model scale, the viscous effects not only dominate the overall instantaneous wake distribution but, they also appear to strongly affect the time-varying part of the wake field in waves. Based on this, it was concluded that potential flow calculation methods might not be suitable to estimate the time-variation of the nominal wake field in waves in model scale.

However, the viscous effects and their impact on the wake field get progressively less important with increasing Reynolds number. In addition, the influence of the bilge vortex on the propeller inflow is reduced in the effective wake field in full scale compared to the nominal wake field in model scale [22]. Therefore, the new idea is to apply the same approach in full scale rather than in model scale by considering the effective wake field and not the nominal one. Specifically, the effective calm water wake distribution in full-scale is used as base wake field for the method. For the sake of comparison, the effective wake field in calm water is scaled to match the full-scale effective average wake fraction, $w_S = 0.305$, obtained by Kim et al. [13].

The full-scale effective wake field in waves, computed by the described method, is shown in Figure 10. For brevity, the effective wake field in waves is shown only at one time instance for each wave.

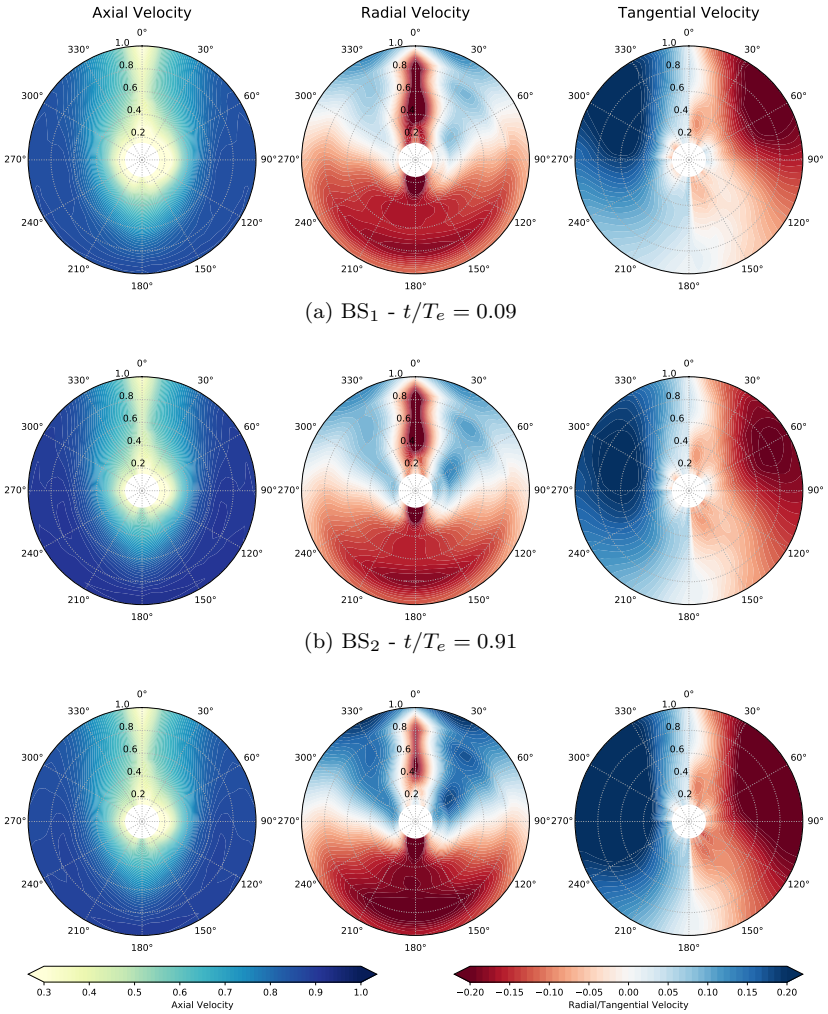

(a) BS_1 - $t/T_e = 0.09$

(b) BS_2 - $t/T_e = 0.91$

(c) BS_3 - $t/T_e = 0.79$

Figure 10: Time-varying effective wake field in full-scale in waves.

As a validation of the method, average wake fractions of the resulting time-varying wake field are compared with average wake fractions estimated as described by Taskar [28]: the time-varying total wake velocity in waves, V_t, is computed by considering a dimensionless mean increase in propeller inflow, V_m, and a fluctuating velocity component, V_f, as follows:

$$V_t = V_f \cdot V_m \tag{1}$$

The fluctuating velocity V_f is computed including the surge motion effect

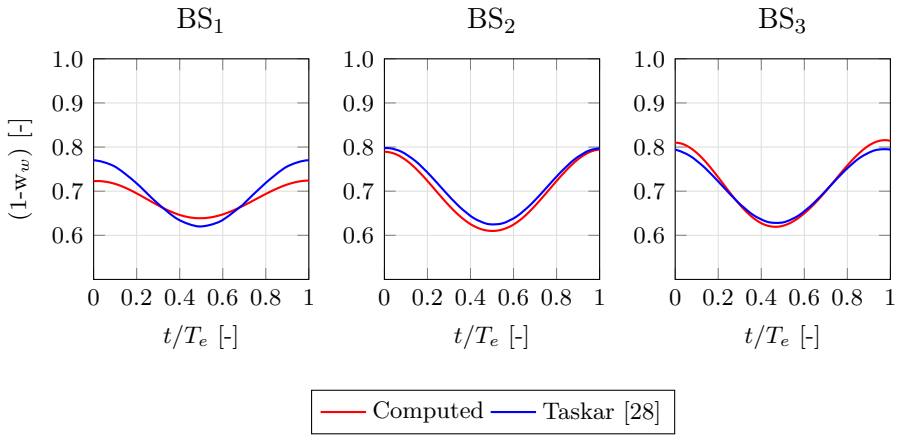

Figure 11: Comparison of effective average wake fractions.

and the orbital motion of water particles in an attenuated wave at the stern, as described by Ueno et al. [33]. The mean increase V_m is computed assuming the bottom of the ship to be a flat plate that is pitching harmonically, as explained by Faltinsen et al. [4].

Figure 11 shows the comparison, for the selected three wavelengths (see Section 5.1.1), between the average wake fractions of the resulting time-varying wake field (red curve) and the average wake fractions estimated as described by Taskar [28] (blue curve). Small differences in the fluctuation amplitude can be noticed for the short wave.

Only the average wake fractions are compared because of the nonavailability of the effective wake distribution in full-scale in waves for the considered cases.

5.1.4. Propeller speed in calm water conditions

The propeller rate of revolutions in calm water conditions is not set equal to the design value of the KP458 propeller, but it is computed by considering the intersection between the required thrust relation K_T/J^2 and the open water thrust coefficient curve K_T. This is performed to be consistent with the computation of the speed loss.

The residual resistance coefficient C_R is obtained by averaging the experimental results provided by Larsson et al. [16]. Measurements were carried out in the MOERI (formerly KRISO) towing tank and the test basin at the University of Osaka.

The friction resistance coefficient C_F is computed by applying the ITTC 57 Model-Ship Correlation Line [8]. The form factors are also provided by Larsson et al. [16].

The propulsion factors were determined experimentally in model scale and extrapolated to full scale by Kim et al. [13].

The propeller rate of revolutions in calm water conditions, estimated with the described method, is equal to 1.176 rps.

5.1.5. Propeller speed fluctuations

An approximated numerical method is applied to compute the propeller speed fluctuations due to the absence of an engine-propeller model for the propulsion system of the KVLCC2 vessel. This method, validated by Taskar [28], determines the variation of the propeller rate of revolution with the assumption of constant torque.

Quasi-steady simulations are performed by ESPPRO, for each time instance, keeping the propeller speed equal to its value in calm water conditions. These simulations are used to compute the temporal mean of the torque in one encounter wave period. For each time instance, the open water curve (KQ-J diagram - see Figure 2) is used to create the torque speed characteristic of the propeller. The propeller speed variation is obtained using the torque speed characteristics and the temporal mean of the torque. This procedure is practical for constant torque machines as marine diesel engines.

The propeller speed fluctuations, estimated with the described method, are shown in Figure. 12.

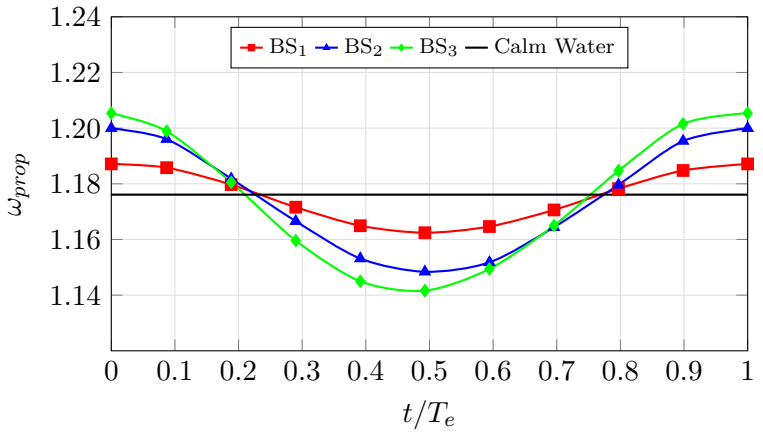

Figure 12: Calm water propeller speed and propeller speed fluctuations.

5.1.6. Speed loss

The classical power prediction approach is applied to compute the speed loss. Generally, in this method, the resistance curve is modified by adding the resistance due to waves, wind, yawing, steering, and other effects to the calm water resistance [26]. For simplicity, only wind resistance and added resistance in waves are considered in the present work.

The calm water resistance curve is computed as described in Section 5.1.4.

The added resistance is calculated in irregular waves even though regular waves are considered. Generally, the added resistance estimated in irregular waves is lower than the corresponding one in regular waves. In the selected case, if the added resistance were computed for regular waves, the new ship speeds would be unrealistically low. Therefore, irregular waves are considered with significant wave heights and peak frequencies equal to the wave heights and frequencies of the regular waves simulated in SHIPFLOW Motions (see Section 5.1.1 and Table. 4). The method described in ITTC [9] is used along with the modified Pierson-Moskowitz wave spectrum to compute the added resistance in irregular waves.

The wind resistance is calculated following the method described in ITTC [9]. The KVLCC2 superstructure is assumed to be located at the aft with dimensions typical for a tanker of that size.

The speed loss in waves, computed with the described method, is shown in Table 5.

Wave [−]	Speed Loss [kts]
BS_1	1.20
BS_2	1.26
BS_3	1.01

Table 5: Speed loss in waves.

5.1.7. Hull pressure pulses

Hull pressure pulses are evaluated by analyzing the time-varying pressure signal computed with the Bernoulli equation.

A common approach for extracting pressure pulse harmonics at blade frequency and their multiples is the Fast Fourier Transform (FFT). This method assumes stationarity of the data in the time-window in which it is applied. This condition is achieved in calm water conditions. However, this

requirement is generally not fulfilled in the presence of waves where data are non-stationary. Therefore, the conversion of the time-varying pressure signal via the FFT cannot be applied. The solution implemented in the present work is to use the Hilbert-Huang Transform (HHT) [7]. Unlike the FFT, the HHT is not constrained by the assumptions of stationarity and computes the amplitude of the signal as a function of time. Compared to the FFT, before applying the HHT, the time-varying pressure signal needs to be filtered to extract the pressure harmonics. The chosen filter is an NTNU-developed pass-band filter, and the cut-off frequencies are dynamically calibrated to isolate the blade frequency and its multiples. The FFT can still be applied in the quasi-steady case where data are stationary. Nevertheless, the HHT is also used in the quasi-steady approach to be consistent with the calculation of the pressure harmonics.

The influence of the hull surface on the pressure pulses is introduced using the concept of solid boundary factor (SBF), which is defined as the ratio between the pressure acting on the boundary surface and the free-field pressure in the absence of the solid boundary at the same location. Specifically, the hull is modeled as a flat plate of infinite stiffness, resulting in an SBF equal to 2.

6. Results and discussion

6.1. Open water condition

Unsteady propeller forces of the KVLCC2 propeller are computed using both the quasi-steady and the fully-unsteady approach.

The comparison shows the same trend for all the considered plane progressive waves. Therefore, for brevity, the variation of K_T and K_Q, over the corresponding wave encounter period, is presented in Figures 13 and 14 only for three representative cases: OW_1, OW_4, and OW_7 (see Table 3).

As explained in Section 1, a quasi-steady simulation provides results only at the selected time instance. As a consequence, for the quasi-steady approach, the unsteady propeller forces are represented over time by dots. On the other hand, results are displayed with a continuous curve for the fully-unsteady approach. Additionally, the discrete-time instances for the quasi-steady calculations are shown as violet vertical lines.

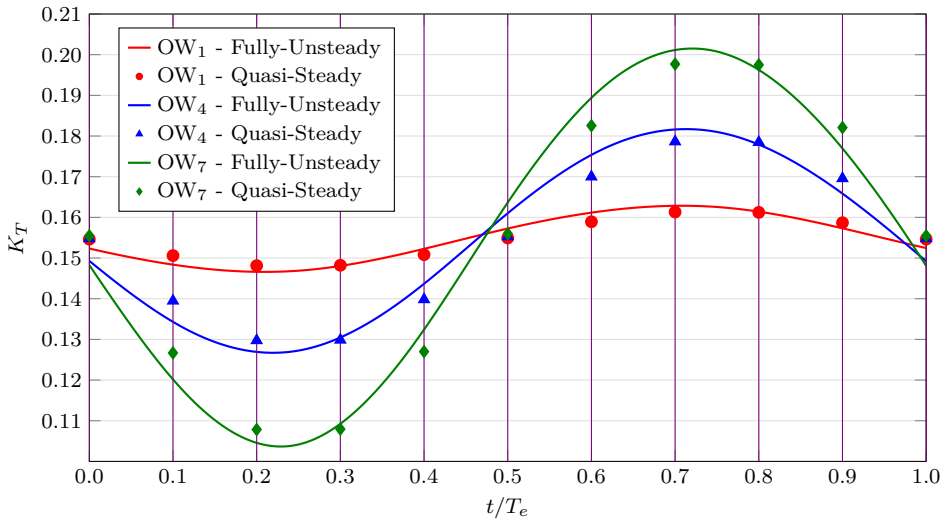

Figure 13: K_T comparison - OW_1, OW_4, and OW_7.

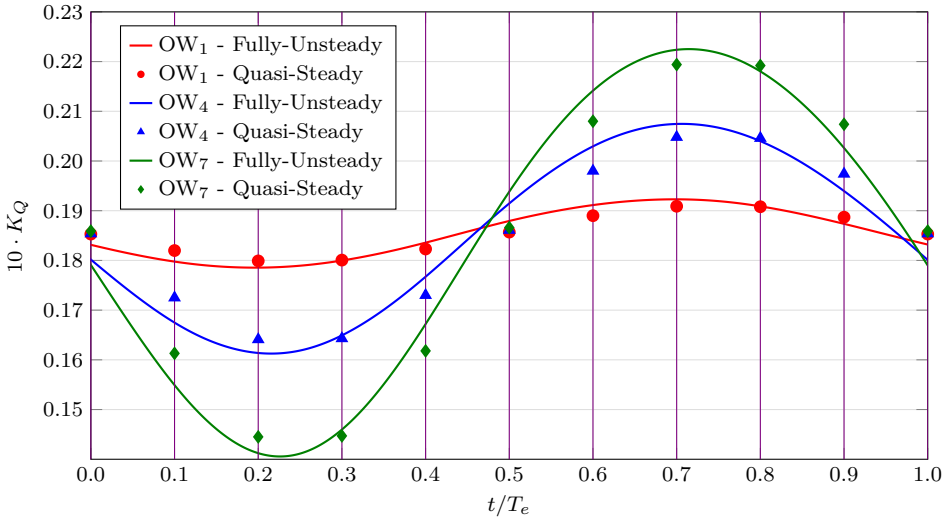

Figure 14: K_Q comparison - OW_1, OW_4, and OW_7.

Figures 13 and 14 show a good agreement in the amplitudes of K_T and K_Q between the two approaches.

Wave [−]	Max. Rel. Diff. K_T [%]	Max. Rel. Diff. K_Q [%]	ω_{prop_d}/ω_e [−]
OW_1	1.53	1.19	4.77
OW_2	2.39	1.82	5.88
OW_3	3.01	2.37	7.02
OW_4	3.81	2.99	8.17
OW_5	4.22	3.29	9.35
OW_6	4.56	3.58	10.53
OW_7	4.83	3.78	11.73

Table 6: Maximum relative difference of K_T and K_Q.

On the other hand, notable differences can be seen when comparing the unsteady propeller forces at the discrete-time instances. Table 6 shows the maximum relative difference of K_T and K_Q, for each progressive wave, between the two approaches. It can be noticed that the higher the ratio of propeller angular frequency to wave encounter frequency, the higher the maximum difference between the quasi-steady and the fully-unsteady approach. This is not in line with the hypothesis formulated to justify why the quasi-steady approach can be used to substitute the fully-unsteady approach: the ratio of propeller angular frequency to wave encounter frequency needs to be sufficiently large. This is because, in general, the influence of the time history of the propeller performance on the prediction of the unsteady propeller forces also depends on the amplitude of the fluctuation of the time-varying input data and on how quickly these time-varying input data change in time. In other words, for the considered case, the difference between the two approaches increases with the increasing magnitude of the acceleration of the time-varying wake field. This can be seen from the particle acceleration amplitude of the plane progressive waves, computed at the design value of the shaft submergence, shown in Table 7.

Wave [−]	Acceleration amplitude $[m/sec^2]$
OW_1	0.227
OW_2	0.356
OW_3	0.476
OW_4	0.581
OW_5	0.671
OW_6	0.745
OW_7	0.807

Table 7: Particle acceleration amplitude of the plane progressive waves.

The quasi-steady and the fully-unsteady approach have the same wake blade geometry and propeller wake field at the same time instance. As a consequence, the difference in unsteady propeller forces, between the two approaches, is mainly related to the memory effect of the shed vorticity in the blade wake. This also explains the trend of the difference in unsteady propeller forces between the two approaches for the same plane progressive wave. Let's consider K_T (see Figure 13), for one plane progressive wave, at the two time instances t/T_e=0.2 and t/T_e=0.3. The axial wake field and the blade wake geometry are the same for these instants of time. Thus, it is possible to assert that, for the quasi-steady approach, the thrust generated by the propeller at t/T_e=0.2 and t/T_e=0.3 is almost the same. However, for the fully-unsteady approach, the memory effects experienced by the two time instances are different. This is related to the particle acceleration of the plane progressive wave, shown in Figure 15. The memory effect for t/T_e=0.2 is related to its previous time instances where the magnitude of the acceleration is higher than the magnitude of the acceleration of the previous time instances of t/T_e=0.3. Therefore, at t/T_e=0.2 the memory effect of the shed vorticity in the blade wake has a higher impact than the one at t=0.3. This explains the higher difference in K_T at t/T_e=0.2 than at t/T_e=0.3 between the quasi-steady and the fully unsteady approach.

Consequently, for the same plane progressive wave, the impact of the memory effect on the difference between the quasi-steady and the fully-unsteady approach decreases with the decreasing of the advance ratio. This is because, for a given wake field, the higher the propeller load the lower the relative variation in the angle of attack caused by the time-varying wake field.

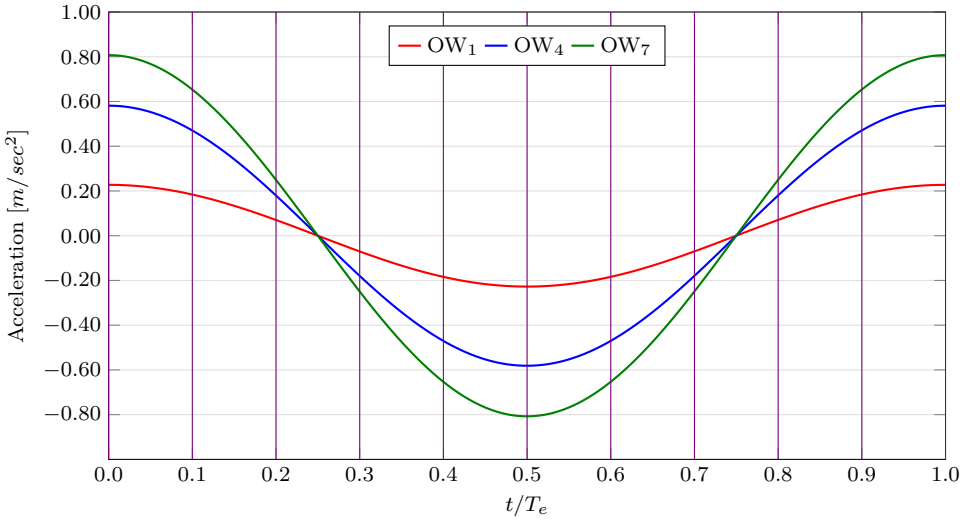

Figure 15: Particle acceleration in the plane progressive wave - OW_1, OW_4, and OW_7.

It is also important to compare the temporal mean of K_T and K_Q, computed over the wave encounter period. This is necessary for the estimation of the mean increase of propeller thrust and torque due to the presence of waves. Table 8 shows negligible differences, between the two approaches, for all the considered plane progressive waves.

Wave [−]	Rel. Diff. K_T [%]	Rel. Diff. K_Q [%]
OW_1	0.14	0.10
OW_2	0.18	0.13
OW_3	0.21	0.14
OW_4	0.21	0.13
OW_5	0.21	0.12
OW_6	0.19	0.09
OW_7	0.17	0.06

Table 8: Relative temporal mean difference of K_T and K_Q.

6.2. Behind ship condition

Unsteady propeller forces, cavitation volume, and hull pressure pulses of the KVLCC2 propeller are computed using both the quasi-steady and the fully-unsteady approach. The propeller performance in calm water conditions is also estimated to quantify the importance of the difference in prediction between the two approaches.

6.2.1. Unsteady propeller forces

Figures 16–21 show the variation of K_T and K_Q over an entire wave encounter period. Results are presented in red for the quasi-steady approach, blue for the fully-unsteady approach and green for the calm water conditions. Additionally, the discrete-time instances for the quasi-steady calculations are displayed as violet vertical lines.

The propeller speed fluctuations lead to a comparison where, for each time instance, the quasi-steady and the fully-unsteady approach have, generally, the same time-varying input data but different position of the propeller blades. This issue makes it difficult to compare the unsteady propeller forces over time between the quasi-steady and the fully-unsteady approach. The solution implemented to overcome this problem consists of plotting the quasi-steady results in sub-domains centered at the corresponding time instances. First and last value of each sub-domain are selected to be in the middle of two adjacent time instances. This technique creates a discontinuous piecewise function defined in a domain equal to the corresponding wave encounter period. This type of representation provides a general overview of the discrepancies between the two approaches over the whole wave encounter period.

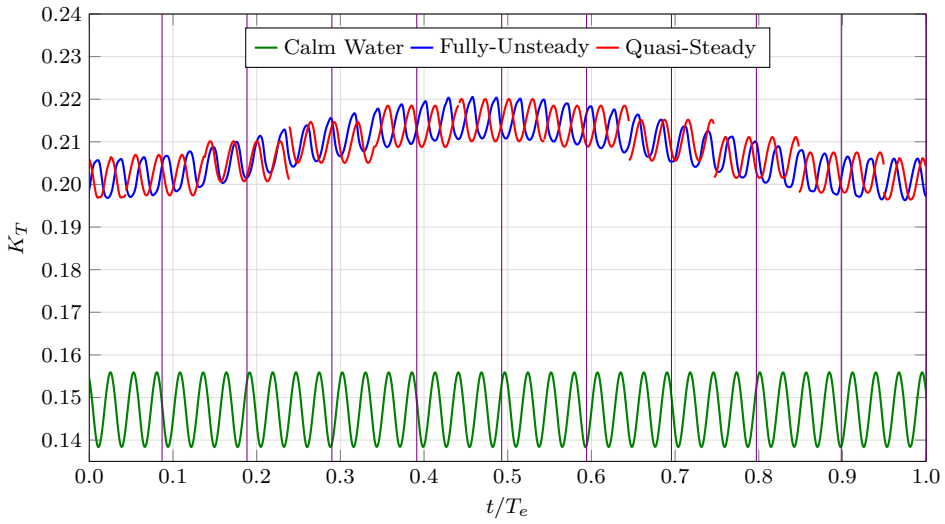

Figure 16: K_T comparison - BS_1 - $J_{wave} = 0.332$ - $J_{calm} = 0.478$

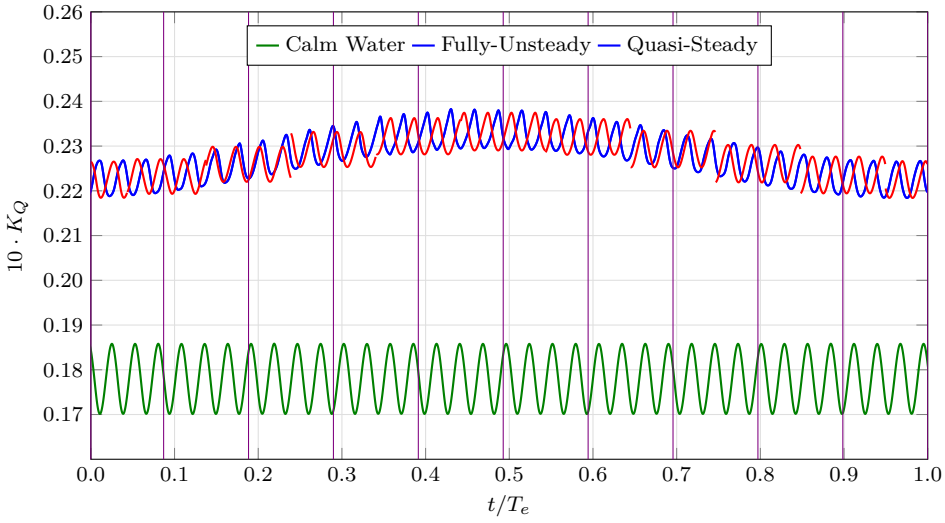

Figure 17: K_Q comparison - BS_1 - $J_{wave} = = 0.332$ - $J_{calm} = 0.478$

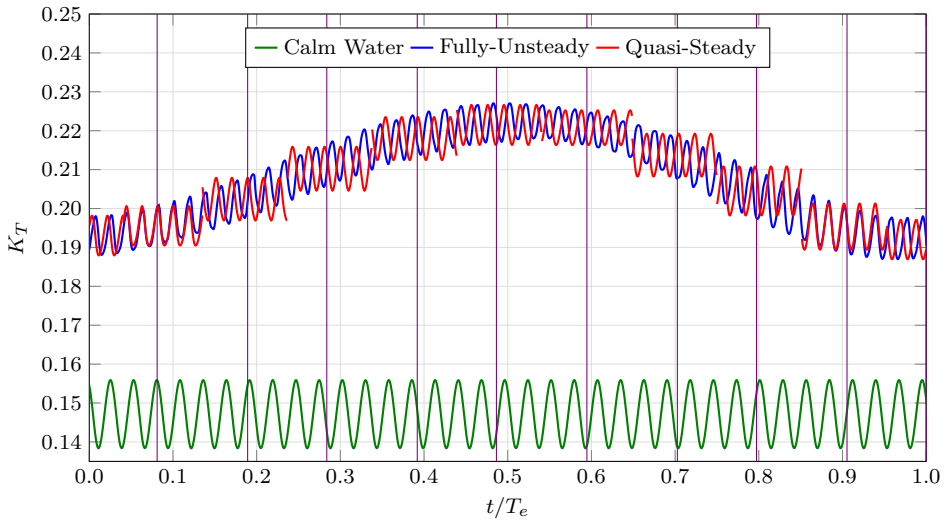

Figure 18: K_T comparison - BS_2 - $J_{wave} = 0.333$ - $J_{calm} = 0.478$

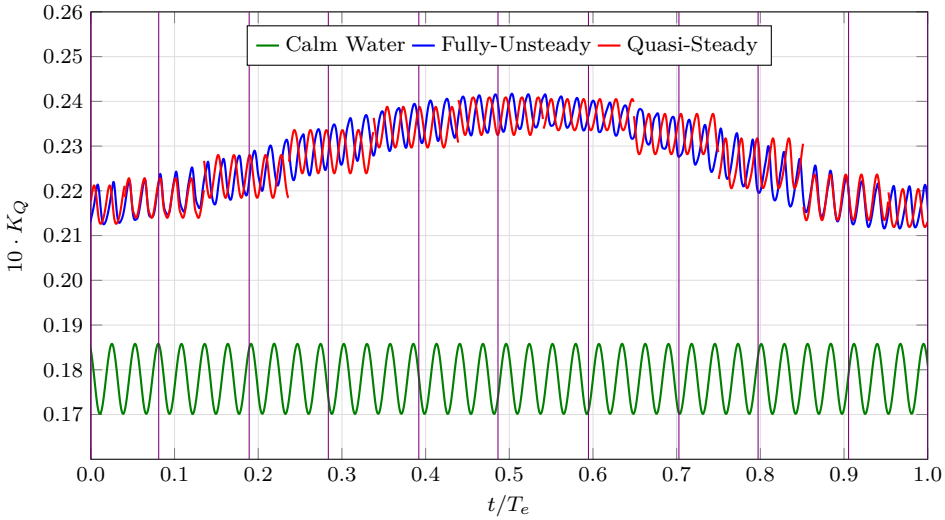

Figure 19: K_Q comparison - BS_2 - $J_{wave} = 0.333$ - $J_{calm} = 0.478$

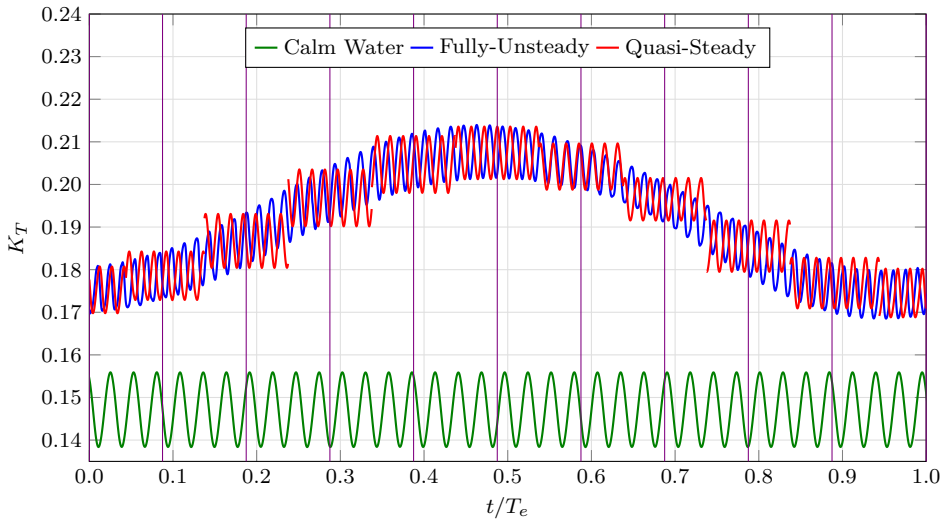

Figure 20: K_T comparison - BS_3 - $J_{wave} = 0.372$ - $J_{calm} = 0.478$

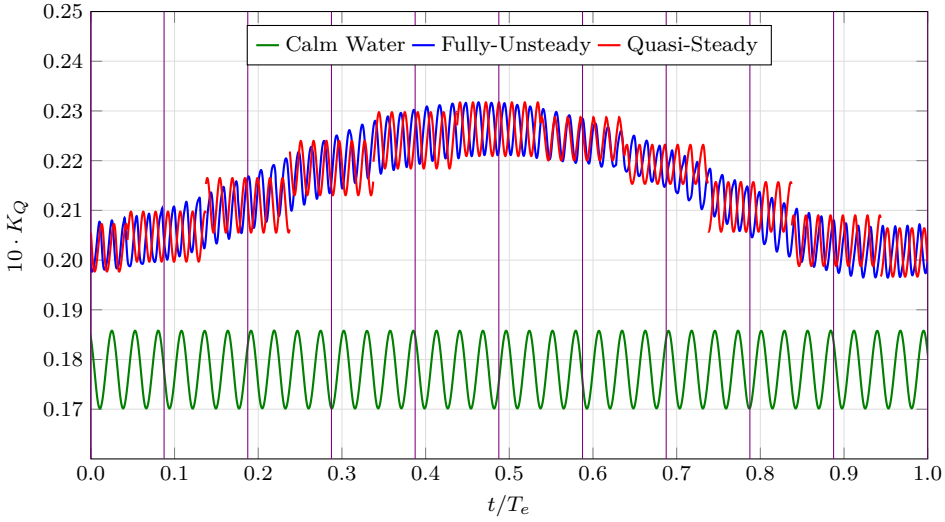

Figure 21: K_Q comparison - BS_3 - $J_{wave} = 0.372$ - $J_{calm} = 0.478$

Figures 16–21 show a good agreement in the low frequency amplitude of K_T and K_Q between the two approaches. This finding confirms the results presented in Section 6.1.

Negligible differences in unsteady propeller forces over time between the quasi-steady and the fully-unsteady approach can be also noted. The reason

Wave [−]	Rel. Diff. K_T [%]	Rel. Diff. K_Q [%]
BS_1	0.02	0.01
BS_2	0.16	0.12
BS_3	0.12	0.08

Table 9: Relative temporal mean difference of K_T and K_Q.

for this is that the high propeller load, caused by the added resistance, leads to a relatively low variation of the angle of attack and, it reduces the difference over time between the quasi-steady and the fully-unsteady approach (also see Section 6.1).

Table 9 shows a negligible difference in the temporal mean of K_T and K_Q, computed over the wave encounter period, between the quasi-steady and the fully-unsteady approach. This finding confirms the results presented in Section 6.1.

Based on these results, it is possible to conclude that, for the selected case, the unsteady propeller forces predicted by the quasi-steady and the fully-unsteady are in good agreement.

6.2.2. Cavitation volume

Figures 22–24 show the variation of the cavity volume for the key blade over the propeller blade angle.

Results are presented in red for the quasi-steady approach and blue for the fully-unsteady approach. Additionally, the blade angle corresponding to the time instances for the quasi-steady calculations are displayed as violet vertical lines. The cavity volume is nondimensionalized by dividing its absolute value to the maximum value of the cavity volume in calm water conditions.

The cavity volume is shown over the propeller blade angle because the position of the blades is the key parameter to compare the quasi-steady and the fully-unsteady approach when considering cavitation. However, for each blade position, the time-varying input data are not the same for the two methods. This comparison is valid as long as the propeller speed fluctuations are moderate compared to the variation in time of the time-varying input data, as in the present case.

The same principle implemented to plot the quasi-steady propeller forces, i.e. quasi-steady results shown in sub-domains centered at the blade angles corresponding to the quasi-steady time instances, is not applied for

the cavity volume. This is because the quasi-steady peaks are located at the corresponding blade angle instances and not where the cavitation peaks of the fully-unsteady approach are. As a consequence, that type of comparison would not be accurate if the difference in blade angle between a quasi-steady and fully-unsteady peak was too high or if the change in cavitation volume in time was too quick. The best possible solution to overcome this issue consisted of synchronizing the quasi-steady angle instances with the cavitation peaks of the fully-unsteady approach. A similar result can be achieved by interpolating the cavitation peaks of the quasi-steady approach, located at the corresponding angle instances, over the encounter wave period. This envelope, presented in red in Figures 22–24, makes it possible to compare the variation in time of the cavitation peaks between the quasi-steady and the fully-unsteady approach.

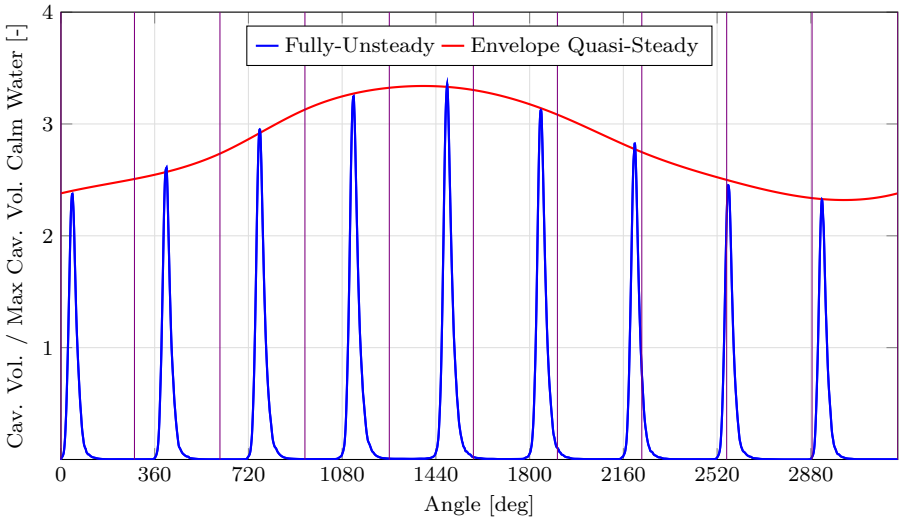

Figure 22: Calm water - Cavity volume key blade - BS_1.

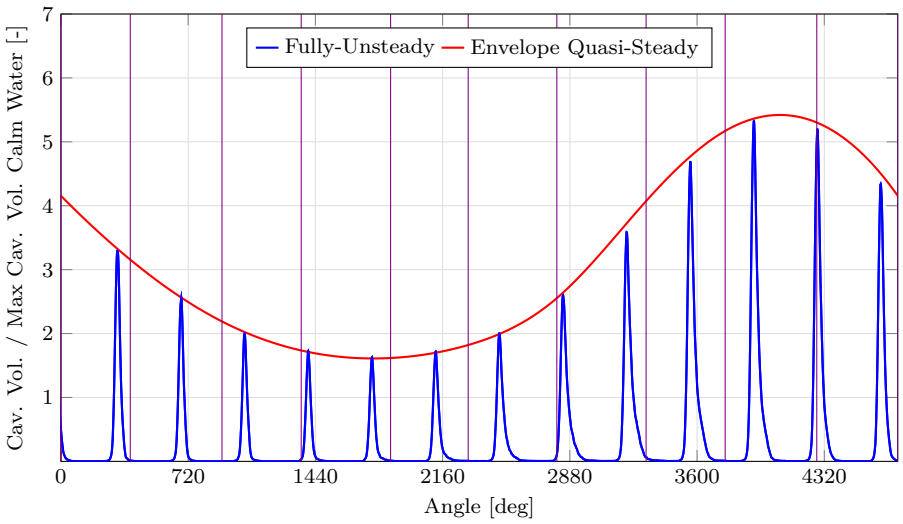

Figure 23: Calm water - Cavity volume key blade - BS_2.

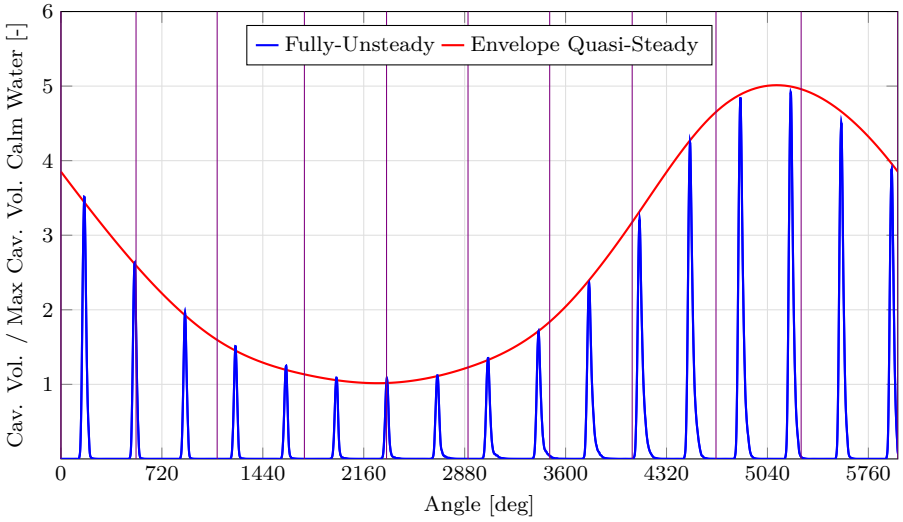

Figure 24: Calm water - Cavity volume key blade - BS_3.

Figures 22–24 show a negligible difference in maximum cavity volume between the quasi-steady and the fully-unsteady approach. This outcome is mainly related to the good agreement in unsteady propeller forces (see Section 6.2.1) and to the moderate time-variation of the shaft submergence (see Figure 8).

Therefore, it is possible to conclude that, for the selected case, the cavity volume predicted by the quasi-steady and the fully-unsteady is in good agreement.

6.2.3. Hull pressure pulses

The comparison in propeller-induced pressure pulses between the full-unsteady and the quasi-steady approach shows a similar trend for the three considered waves. Thus, for brevity, results are only presented for one representative case: BS_2 at t/T_e= 0.59.

Figure 25 shows the first three harmonics of the hull pressure pulses for the nine selected points (also see Section 5).

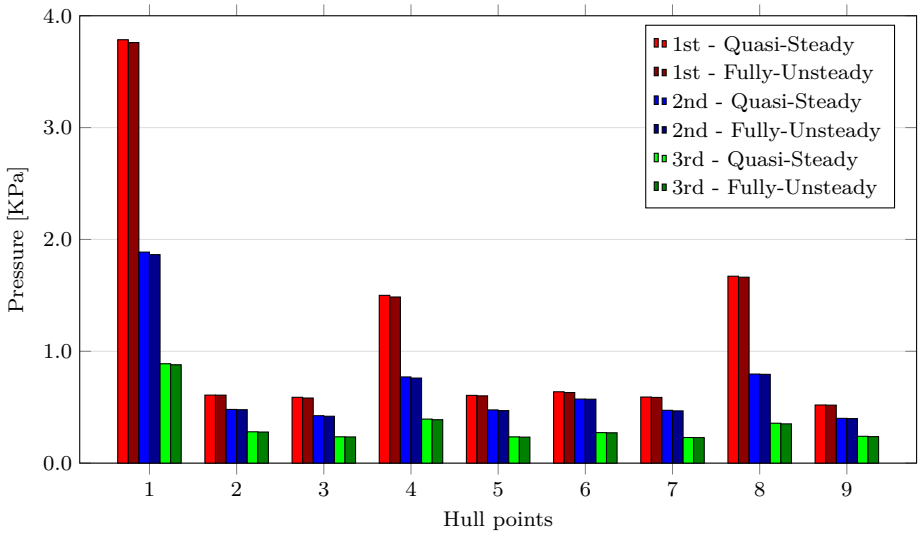

Figure 25: Hull pressure pulses - BS_2 - t/T_e= 0.59

Figure 25 shows a negligible difference in propeller-induced pressure pulses between the quasi-steady and the fully-unsteady approach. This outcome is mainly related to the good agreement in unsteady propeller forces (see Section 6.2.1) and in cavitation volume (see Section 6.2.2).

As a result, it is possible to conclude that, for the selected case, the hull pressure pulses predicted by the quasi-steady and the fully-unsteady are in good agreement.

7. Conclusion

The quasi-steady and a fully-unsteady approach were compared by computing the propeller performance of the KVLCC2 in the presence of waves.

First, a simple comparison in open water head waves was carried out to quantify the differences in unsteady propeller forces between the two approaches. The comparison showed a small difference in the temporal mean and in the fluctuation amplitude of K_T and K_Q, computed over the encounter wave period.

Second, the results obtained from the first comparison were confirmed by considering three realistic case scenarios for the KVLCC2 when sailing in head sea conditions. The comparison showed insignificant differences in the temporal mean and in the fluctuation amplitude of K_T and K_Q, computed over the encounter wave period. Negligible differences were observed in cavity volume variation and hull pressure pulses.

Based on these results, it is possible to conclude that, for the considered operating conditions, the temporal mean and the fluctuation amplitude of K_T and K_Q, the cavity volume variation, and the hull pressure pulses predicted by the quasi-steady and the fully-unsteady are in good agreement.

Appendix A.

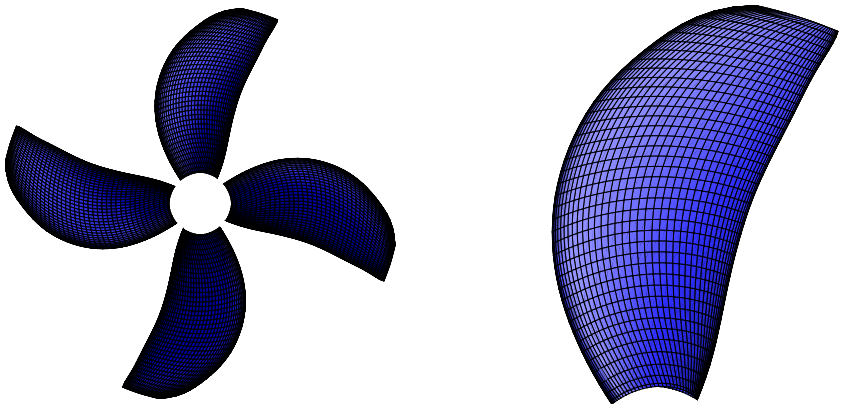

Figure A.26: Propeller grid for the propeller analysis (see Section 2 and 5.1.2).

Appendix B.

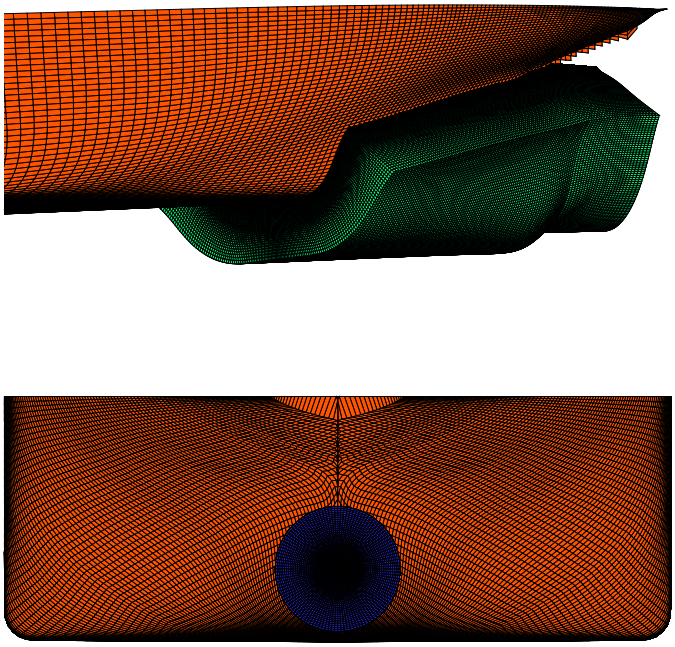

Figure B.27: Details of the grid used in the RANS calculations (see Section 5.1.2).

Appendix C.

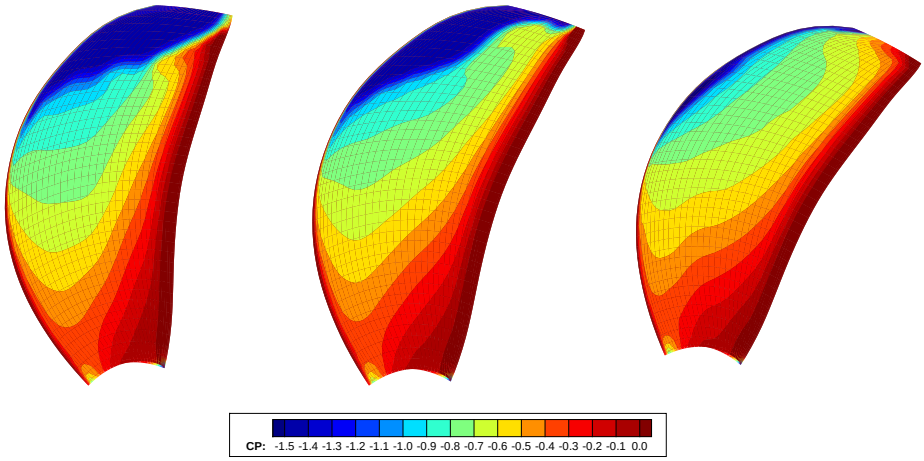

Figure C.28: Suction side pressure distribution at -10° (left), 12 O'clock (center), and +10° (right) for the full-scale effective wake field in calm water - $C_P = \frac{P}{\rho n^2 D^2}$ (see Section 5.1.2).

References

[1] Chevalier, Y. and Kim, Y. H. (1995). Propeller Operating in a Seaway. In *PRADS'95*.

[2] Dallinga, R., Flikkema, M., and Grin, R. (2008). Challenging wind and waves-their impact on fuel consumption. *MARIN report*, 94:1–3.

[3] Faltinsen, O. M. (2005). *Hydrodynamics of high-speed marine vehicles*. Cambridge university press.

[4] Faltinsen, O. M., Minsaas, K. J., Liapis, N., and Skjordal, S. O. (1980). Prediction of Resistance and Propulsion of a Ship in a Seaway. *13th Symposium on Naval Hydrodynamics*, pages 505–529.

[5] Guo, B. J., Steen, S., and Deng, G. B. (2012). Seakeeping prediction of KVLCC2 in head waves with RANS. *Applied Ocean Research*, 35:56–67.

[6] Hoshino, T. (1989). Hydrodynamic Analysis of Propellers in Steady Flow Usinga Surface Panel Method. *Journal of the Society of Naval Architects of Japan*, 1989(166):79–92.

[7] Huang, N. E. (2014). *Hilbert-Huang transform and its applications*, volume 16. World Scientific.

[8] ITTC (2011). Recommended Procedures and Guidelines: Resistance Test.

[9] ITTC (2014). Recommended Procedures and Guidelines: Speed and Power Trials, Part 2 Analysis of Speed/Power Trial Data.

[10] Janson, C. E. (1997). *Potential flow panel methods for the calculation of free-surface flows with lift*. PhD thesis, Chalmers University of Technology.

[11] Jessup, S. D. and Wang, H. C. (1996). Propeller Cavitation Prediction for a Ship in a Seaway. Technical report, US Naval Surface Warfare Center.

[12] Kim, H., Hayashi, Y., and Oshita, S. (2012). Phase-Averaged SPIV Wake Field Measurement for KVLCC2 Propeller Plane in Waves. , (15):65–68.

[13] Kim, W. J., Van, S. H., and Kim, D. H. (2001). Measurement of flows around modern commercial ship models. *Experiments in fluids*, 31(5):567–578.

[14] Kinnas, S. A. and Fine, N. E. (1993). A numerical nonlinear analysis of the flow around two-and three-dimensional partially cavitating hydrofoils. *Journal of Fluid Mechanics*, 254:151–181.

[15] Kjellberg, M. (2013). *Fully Nonlinear Unsteady Three-Dimensional Boundary Element Method for Ship Motions in Waves*. PhD thesis, Chalmers University of Technology.

[16] Larsson, L., Stern, F., and Visonneau, M. e. (2013). *Numerical ship hydrodynamics: an assessment of the Gothenburg 2010 workshop*. Springer.

[17] Mirsadraee, Y. (2018). *Development of a Model for Propeller Tip Vortex Cavitation and Analysis of the Radiated Pressure Fluctuations*. PhD thesis, Technical University of Denmark (DTU).

[18] Moeri (2008). KVLCC2 Propeller (MOERI). `http://www.simman2008.dk/KVLCC/KVLCC2/kvlcc2_geometry.html`. Online; accessed: 01.07.2019.

[19] Moor, D. I. and Murdey, D. C. (1970). Motions and Propulsion of Single Screw Models in Head Seas, Part II. *Quarterly Transactions of the Royal Institution of Naval Architects*, 112(2):121–127.

[20] Nakamura, S. and Naito, S. (1977). Propulsive performance of a container ship in waves. *Journal of the Society of Naval Architects of Japan*, 15.

[21] Regener, P. B. (2016). *Hull-Propeller Interaction and Its Effect on Propeller Cavitation*. PhD thesis, Technical University of Denmark.

[22] Regener, P. B., Mirsadraee, Y., and Andersen, P. (2018). Nominal vs. effective wake fields and their influence on propeller cavitation performance. *Journal of Marine Science and Engineering*, 6(2):34.

[23] Rodrigue, J., Comtois, C., and Slack, B. (2016). Transportation modes, modal competition and modal shift. *The Geography of Transport Systems.(come from: https://transportgeography. org/)*.

[24] Sadat-Hosseini, H., Wu, P. C., Carrica, P. M., Kim, H., Toda, Y., and Stern, F. (2013). CFD verification and validation of added resistance and motions of KVLCC2 with fixed and free surge in short and long head waves. *Ocean Engineering*, 59:240–273.

[25] Smith, T. W. P., Jalkanen, J. P., Anderson, B. A., Corbett, J. J., Faber, J., Hanayama, S., O'keeffe, E., Parker, S., Johanasson, L., Aldous, L., et al. (2015). Third IMO GHG Study.

[26] Steen, S. and Chuang, Z. (2013). Measurement of speed loss due to waves. In *3rd International Symposium on Marine Propulsors (smp'13)*, pages 439–446, Launceston, Australia.

[27] Streckwall, H. (1998). Hydrodynamic analysis of three propellers using a surface panel method for steady and unsteady inflow conditions. In *22nd ITTC Propulsion Committee Propeller RANS/Panel Method Workshop*, Grenoble, France.

[28] Taskar, B. (2017). *The Effect of Waves on Marine Propellers and Propulsion*. PhD thesis, Norwegian University of Science and Technology.

[29] Taskar, B., Steen, S., Bensow, R. E., and Schröder, B. (2016a). Effect of waves on cavitation and pressure pulses. *Applied Ocean Research*, 60:61–74.

[30] Taskar, B., Steen, S., and Eriksson, J. (2017). Effect of waves on cavitation and pressure pulses of a tanker with twin podded propulsion. *Applied Ocean Research*, 65:206–218.

[31] Taskar, B., Yum, K. K., Steen, S., and Pedersen, E. (2016b). The effect of waves on engine-propeller dynamics and propulsion performance of ships. *Ocean Engineering*, 122:262–277.

[32] Tian, Y. and Kinnas, S. A. (2012). A wake model for the prediction of propeller performance at low advance ratios. *International Journal of Rotating Machinery*, 2012.

[33] Ueno, M., Tsukada, Y., and Tanizawa, K. (2013). Estimation and prediction of effective inflow velocity to propeller in waves. *Journal of Marine Science and Technology*, 18(3):339–348.

[34] Vaz, G., Hally, D., Huuva, T., Bulten, N., Muller, P., Becchi, P., Herrer, J. L., Whitworth, S., Macé, R., and Korsström, A. (2015). Cavitating flow calculations for the E779A propeller in open water and behind conditions: code comparison and solution validation. In *Proceedings of the 4th International Symposium on Marine Propulsors (smp'15), Austin, TX, USA*, pages 330–345.

[35] Vaz, G. N. V. B. and Bosschers, J. (2006). Modelling three dimensional sheet cavitation on marine propellers using a boundary element method. In *Proceedings of the Sixth International Symposium on Cavitation, Wageningen, The Netherlands*, pages 11–15.

Conflict of Interest and Authorship Conformation Form

All authors have participated in (a) conception and design, or analysis and interpretation of the data; (b) drafting the article or revising it critically for important intellectual content; and (c) approval of the final version.

This manuscript has not been submitted to, nor is under review at, another journal or other publishing venue.

The authors have no affiliation with any organization with a direct or indirect financial interest in the subject matter discussed in the manuscript.